Optical Transfer Function of Concave Grating Spectrometer Based on Wave Optical Method

Optical Transfer Function of Concave Grating Spectrometer Based on Wave Optical Method

Tsuneo KATAYAMA and Akio TAKAHASHI

Dept. of Mathematics and Physics, the Defense Academy, Yokosuka

(Received March 30, 1970)

Optical transfer functions (OTF) of two types of spectrometer — Eagle mounting and Seya-Namioka mounting — are calculated by the wave-optical method which defines the OTF as the autocorrelation function of the pupil. Results obtained are compared with previous results of the present authors and interpreted as effects of diffraction and aberration on the broadening of point image. The OTFs are calculated also by Fourier transformation of the intensity distribution of point image and compared with those obtained by the first method.

§ 1. Introduction

Aberrations of grating spectrometers have been studied by Beutler's method,[1] in which the light path function is expanded in terms of variables corresponding to width and height of grating, and according to Fermat's principle its terms are made equal to zero in turn. Image performance of spectrometers has been evaluated by a spot diagram as a result of ray tracing[2,3] or by an intensity distribution of point image.[4,5]

On the other hand, the optical transfer function (OTF) gives a powerful means to evaluate image performance of an optical system, and it has been applied to lens systems in many ways. Lohmann[6] applied the OTF to the plane grating with various kinds of ruling errors. The OTFs of the two spectrometers mounted according to Eagle's and Seya-Namioka's principle were calculated by Fourier transformation of the spot diagram obtained by ray tracing.[7] This treatment based on geometrical optics is allowable only if the spectrometers have considerable amount of aberrations. However, when the spectrometers have an extremely small amount of aberrations or when the region of higher spatial frequency is considered, the OTF based on wave optics must be adopted.

A standard method of calculating the OTF is the Fourier transformation of the intensity distribution of point image obtained from Fresnel-Kirchhoff diffraction integral. But a formidable amount of calculation is needed because the method contains two steps of complicated integral. Therefore, in this paper, the wave optical OTFs of spectrometers are calculated from the autocorrelation function of a pupil. Effects of diffraction and aberration on the OTF of the spectrometers are studied by comparison of the present result with the previous one.

§ 2. Method of Computation

2-1 *OTF of spectrometer*

Figure 1 shows a coordinate system adopted in the following. Let $W(x, y)$ be the wavefront aberration at a point (x, y) on the pupil, then the OTF of an optical system can be expressed by means of the well-known formula,

$$D(s,t)=\frac{1}{A}\iint_{-\infty}^{+\infty}\exp\left[ik\left\{W\left(x+\frac{s}{2},y+\frac{t}{2}\right)-W\left(x-\frac{s}{2},y-\frac{t}{2}\right)\right\}\right]dx\,dy, \quad (1)$$

where (x, y) and (s, t) are normalized coordinates on the pupil plane and spatial frequency variables respectively. In applying this formula to a spectrometer, we use actual coordinates (w, l) on the grating surface and actual spatial frequency ν. Since a slit is used as an object in the spectrometer, only the one dimensional spatial frequency is considered. Therefore we have

$$D(\nu)=\frac{1}{P_0}\iint_{P_N}\exp\left[ik\left\{W\left(w+\frac{\lambda\nu r'}{2},l\right)-W\left(w-\frac{\lambda\nu r'}{2},l\right)\right\}\right]dw\,dl, \quad (2)$$

where P_0 is the total area of the grating, P_N is the area common to two pupils displaced relatively each other, λ the wavelength of

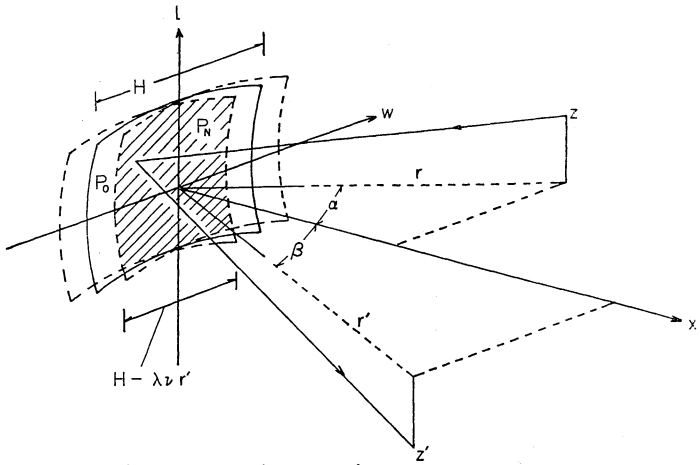

Fig. 1. Coordinate system for a grating spectrometer. The shaded portion represents the region of integration which is common to two pupils displaced relatively each other.

light and r' the distance between grating vertex and image plane. Namioka[4] reported that the intensity distribution of the point image in the horizontal direction w is hardly affected by integration related to l. Accordingly, the integration related to l is neglected in the following calculation. Namely, we consider only the bundle of rays originating from the object point and lying on the Rowland circle plane. Therefore, eq. (2) becomes

$$D(\nu)=\frac{1}{H}\int_{-(H-\lambda\nu r')/2}^{+(H-\lambda\nu r')/2}\exp\left[ik\left\{W\left(w+\frac{\lambda\nu r'}{2}\right)-W\left(w-\frac{\lambda\nu r'}{2}\right)\right\}\right]dw\,, \tag{3}$$

where H represents the grating width.

The wave-front aberration W is defined as the optical distance between a real wave-front and the reference sphere. The relation between ray aberration and wave-front aberration has been given by Hopkins.[8] Let the ideal image point by the grating be the center of reference sphere which passes through the grating vertex, then the radius of reference sphere is equal to r'. Therefore, the ray aberration Δp is given by

$$\Delta p=-\frac{r'}{\cos\beta}\frac{\partial W}{\partial w}\,, \tag{4}$$

where β is the diffraction angle of the principal ray. According to Beutler, on the other hand, the derivative of the light path function F with respect to w, that is $\partial F/\partial w$, corresponds to the angle between the ray through the ideal image point and that of the real one. Thus, the ray aberration of grating is given by

$$\Delta p=R\frac{\partial F}{\partial w}\,. \tag{5}$$

If the light path function for the principal ray is denoted by F_0, we obtain

$$W=-(F-F_0)\,. \tag{6}$$

The light path function of spectrometer with a long slit was given by Miyake and Katayama[9] as

$$\begin{aligned}W(w)=&\left[-\left\{\sin\alpha\left(1+\frac{z^2}{r^2}\right)^{-1/2}+(r',z',\beta)\right\}+\frac{m\lambda}{d}\right]w-\frac{1}{2}\left[\left(1+\frac{z^2}{r^2}\right)^{-3/2}\left\{\frac{\sin^2\alpha}{r}-\left(1+\frac{z^2}{r^2}\right)\left(\frac{1}{r}-\frac{\cos\alpha}{R}\right)\right\}+(r',z',\beta)\right]w^2\\&+\frac{1}{2}\left[\frac{\sin\alpha}{r}\left(1+\frac{z^2}{r^2}\right)^{-5/2}\left\{\left(1+\frac{z^2}{r^2}\right)\times\left(\frac{1}{r}-\frac{\cos\alpha}{R}\right)-\frac{\sin^2\alpha}{r}\right\}+(r',z',\beta)\right]w^3\\&-\frac{1}{8}\left(1+\frac{z^2}{r^2}\right)^{-7/2}\left[\frac{5\sin^4\alpha}{r^3}-\left(1+\frac{z^2}{r^2}\right)\times\left(\frac{1}{r}-\frac{\cos\alpha}{R}\right)\left\{\frac{6\sin^2\alpha}{r^2}-\frac{1}{r}\left(1+\frac{z^2}{r^2}\right)\times\left(\frac{1}{r}-\frac{\cos\alpha}{R}\right)+\frac{1}{R^2}\left(1+\frac{z^2}{r^2}\right)^2\right\}\right]w^4\\&-\frac{1}{8}(r',z',\beta)w^4+\cdots\\=&a_1w+a_2w^2+a_3w^3+a_4w^4+\cdots\,,\end{aligned} \tag{7}$$

where z is the coordinate along the entrance slit, *i.e.* the height of the object point and z'

is the corresponding height of image point, d the grating constant, m the diffraction order and R the radius of curvature of the concave grating. Substituting (7) into (3) and introducing $s'=\lambda r'\nu/2$, we have

$$\begin{aligned}\phi(w)&=W(w+s')-W(w-s')\\&=A_0+A_1w+A_2w^2+A_3w^3+\cdots .\end{aligned}\quad(8)$$

The coefficients A_j are given by

$$\left.\begin{aligned}A_0&=2s'(a_1+a_3s'^2)\\A_1&=4s'(a_2+2a_4s'^2)\\A_2&=6a_3s'\\A_3&=8a_4s'\end{aligned}\right\}.\quad(9)$$

And finally we obtain

$$D(\nu)=\frac{1}{H}\int_{-(H/2-s')}^{(H/2-s')}\exp ik\phi(w)dw\,.\quad(10)$$

If an error smaller than the wavelength is tolerable, it is found that the terms in (7) higher than the fifth order in w can be neglected. Thus, the terms in (8) up to the third order must be retained.

2-2 *Linear approximation of* $\phi(w)$

The exponential part of integrand of (10) is a complex function of the third order, and the integration of this type is analytically difficult. Therefore, the following approximation is introduced.

The surface of the grating is divided into many strips of width Δw. In each strip, $\phi(w)$ is replaced by an equation of straight line tangent to $\phi(w)$, and the integration is performed by a trapezoidal approximation. Stephan[5] calculated the intensity distribution of a point image by a similar method. The value of width Δw is determined by the requirement that the difference between $\phi(w)$ and its tangent $\phi_L(w)$ at w must remain below a tolerance limit ε. This value of ε is determined in advance by a separate experiment. At the lower edge w_j of one divided range, the following condition is derived from the above requirement $|\phi(w_j+\Delta w)-\phi_L(w_j+\Delta w)|=\varepsilon$,

$$|A_3\Delta w^3+(A_2+3A_3w_j)\Delta w^2|=\varepsilon\,.\quad(11)$$

The value of Δw is determined from this equation of the third order in Δw. Among the possible solutions, that of positive and minimum magnitude is automatically selected by the computer as Δw. The value of integral ΔD_j performed in this range is

$$\begin{aligned}\Delta D_j(\nu)&=\int_{w_j}^{w_j+\Delta w}\exp ik[\phi'(w_j)(w-w_j)\\&\quad+\phi(w_j)]dw=\mathrm{Re}_j+i\,\mathrm{Im}_j\,,\end{aligned}\quad(12)$$

where Re_j and Im_j are

$$\left.\begin{aligned}\mathrm{Re}_j&=\frac{1}{k\phi'(w_j)}[\sin k\phi(w_j+\Delta w)-\sin k\phi(w_j)]\\\mathrm{Im}_j&=\frac{1}{k\phi'(w_j)}[\cos k\phi(w_j)-\cos k\phi(w_j+\Delta w)]\end{aligned}\right\}.\quad(13)$$

Therefore, the modulus $|D(\nu)|$ and phase angle θ of the OTF are given as

$$\left.\begin{aligned}|D(\nu)|&=\frac{1}{H}[(\sum_j \mathrm{Re}_j)^2+(\sum_j \mathrm{Im}_j)^2]^{1/2}\\\tan\theta&=(\sum_j \mathrm{Im}_j)/(\sum_j \mathrm{Re}_j)\end{aligned}\right\}\quad(14)$$

respectively.

2-3 *Preliminaries for different types of mounting*

In this treatise, the OTFs of two types of mounting are studied. One is the Eagle mounting which has good imaging properties and the other is the Seya-Namioka mounting which is convenient for use in the vacuum ultraviolet. These mountings were studied in the previous work[7] from the geometric-optical standpoint.

Let α and β be the incident and diffracted angle respectively, r and r' be the distances from grating vertex to entrance and exit slits respectively. The conditions

$$\left.\begin{aligned}2\sin\alpha&=m\lambda/d\\r&=r'=R\cos\alpha\end{aligned}\right\}\quad(15)$$

are fulfilled by the Eagle mounting. And the Seya-Namioka mounting satisfies the condition

$$\left.\begin{aligned}r&=\frac{-2\cos\alpha_0\sin C}{\sin\beta_0(\cos\alpha_0+\cos\beta_0)-\sin C}R\\r'&=\frac{2\cos\beta_0\sin C}{\sin\alpha_0(\cos\alpha_0+\cos\beta_0)+\sin C}R\end{aligned}\right\},\quad(16)$$

where α_0 and β_0 are the incident and diffracted angle at the center of the intended spectral range, and $C=\alpha_0-\beta_0$. The incident angle for the principal ray of any wavelength is given as

$$\sin\alpha=\frac{1}{2}\left[\frac{m\lambda}{d}+\frac{\sin C}{1+\cos C}\right\{2(1+\cos C)$$

$$-\left(\frac{m\lambda}{d}\right)^2\Big\}^{1/2}\Big]. \tag{17}$$

IBM 360 system is employed to calculate after the above scheme. First, the mounting parameters α, β, r and r' for various λ and z are determined; next a_i are determined. Then, Δw_j, $\phi(w_j)$ and $\Delta D_j(\nu)$ are computed for a given frequency ν. The same procedure is repeated until the whole grating width is covered. The computation time to get one curve of the OTF does not exceed one minute even if the type of mounting and the width of grating are different. It is less than the time needed to calculate the OTF by a method of geometrical optics adopted in the previous work.

§ 3. Results of Computation

Specification of the grating adopted in computation is as follows: Radius of curvature, $R=50$ mm; grating constant, $d=1/600$ mm; order of diffraction, $m=+1$; grating width, $H=20$ mm and 50 mm.

The first problem is to determine the value of ε tolerable to the linear approximation of $\phi(w)$. Figure 2 shows the values of OTFs for various ε. They do not change for $\varepsilon<100$A in the Seya-Namioka mounting, and they are almost constant for all values of ε adopted in the Eagle mounting. Therefore the value of ε is fixed at 100A in all computations. Figure 3 shows an example of the state of linearization of $\phi(w)$.

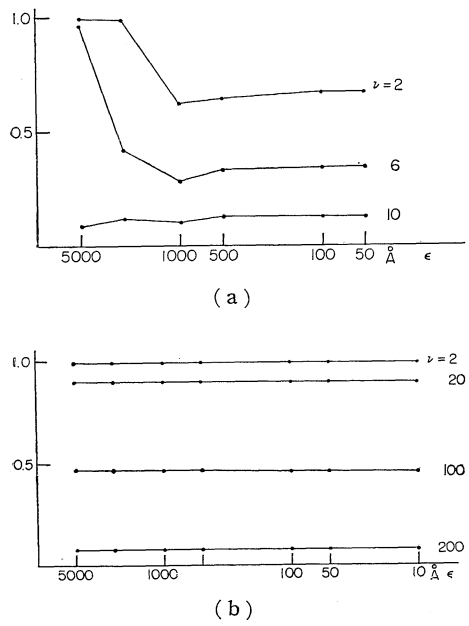

Fig. 2. Values of OTF for various tolerance limits ε and spatial frequencies ν in the case of $H=50$ mm, $z=5$ mm and $\lambda=5461$A. (a) gives the results for Seya-Namioka mounting, (b) gives those for Eagle mounting.

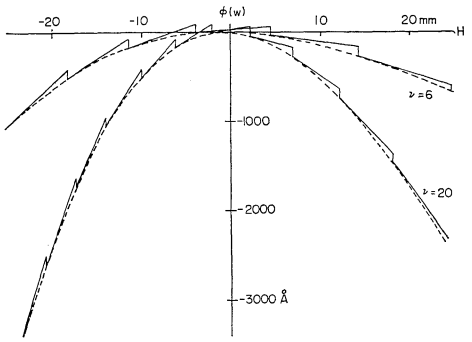

Fig. 3. Results of linearization of $\phi(w)$ in the Seya-Namioka mounting when $\varepsilon=100$A.

The results of the OTF computed by wave optics for the Eagle mounting are shown in Fig. 4. The curve of the OTF shows the following characteristics. With an increase of the grating width, the OTF at the best focal plane extends to higher spatial frequency, but it begins to decrease at lower spatial frequency with an introduction of defocus. This results from the following reason. The Eagle mounting satisfies the Rowland condition at the best focus and has little aberration. In this condition the OTF is substantially determined by diffraction, but as the amount of aberration increases rapidly with defocus, the OTF is principally determined by aberration.

The OTFs for different wavelengths λ are also represented in the figure. The OTF at the best focal plane for a shorter wavelength extends to higher spatial frequency, although it changes little with wavelength at the defocused plane. This result can be understood as follows. At the best focus, the point image reduces in size with decrease of wavelength, but at the defocused plane, the effect of aberration predominates that of diffraction and the difference due to the wavelength becomes negligible.

The results of computation for the Seya-Namioka mounting are given in Fig. 5. It is noted that the OTF at the best focal plane

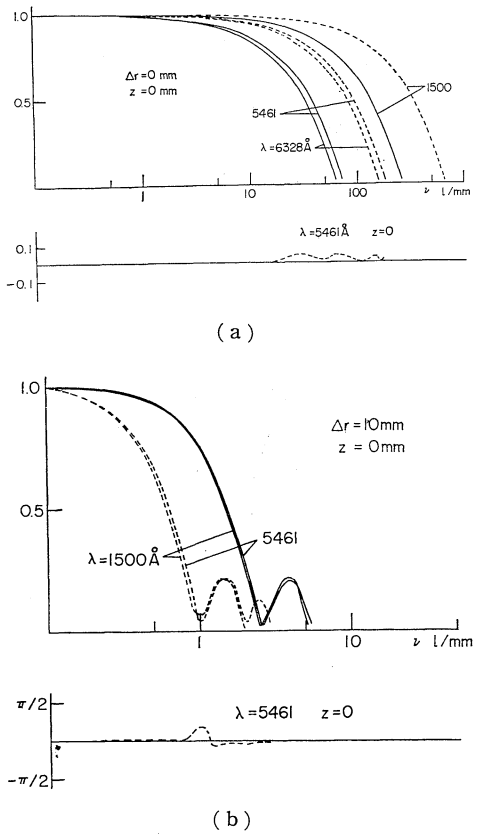

Fig. 4. Modulus and phase of OTFs for Eagle mounting. The full and dotted lines represent OTF when the grating width H=20mm and H =50mm respectively. Δr denotes the amount of defocus.

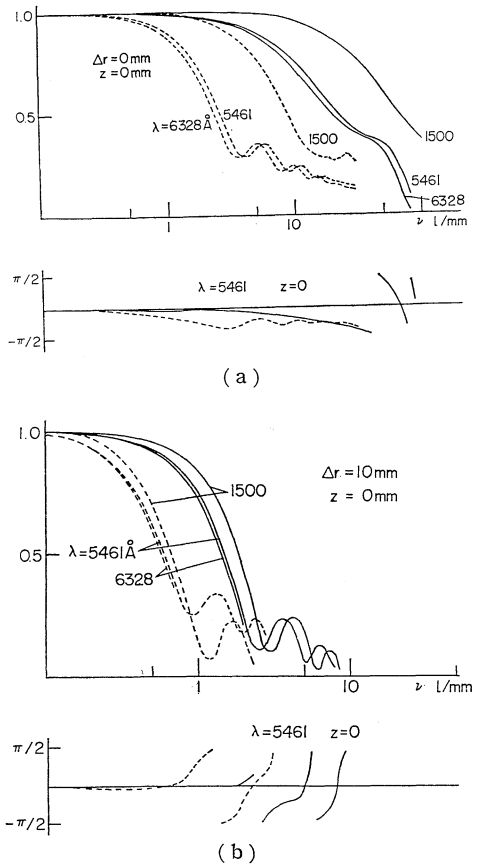

Fig. 5. Modulus and phase of OTFs for Seya-Namioka mounting. The full and dotted lines represent OTF when H=20mm and H=50mm respectively. Δr denotes the amount of defocus.

shows an aspect contrary to that of the Eagle mounting, that is, with a decrease of the grating width, it extends to higher spatial frequency. However, at the defocused plane, it shows a behavior similar to the Eagle mounting. The situation at the best focus comes from the fact that the Rowland condition is not satisfied by the Seya-Namioka mounting for the reason of practical convenience, and there is a considerable amount of aberration even at the best focus. Then, the aberration rather than diffraction has a predominant influence on the OTF. The situation at the defocused plane can be explained in same way as in the Eagle mounting.

The OTFs for different object heights are not shown for both mountings, because no remarkable change of the OTFs does appear.

Figures 6 and 7 show the comparison between the OTFs calculated by the wave optical and the geometric-optical method. When the grating width increases, the curves obtained by both methods have a tendency to become more coincident with each other. This result is reasonable because the approximation of the geometrical optics holds when a system has a considerable amount of aberration or an influence of diffraction can be neglected. The same situation is also found in the case of defocus, in which the agreement is better than at the best focus. But the OTF obtained by the geometrical optics possesses noticeable errors when aberration is small or the spatial frequency is high. Therefore, the computation of the OTF should be carried out by the wave optics in the Eagle mounting which has a small amount of aberration. Moreover, the same conclusion can be derived for the Seya-Namioka mounting, when the OTF is calculated at a considerably

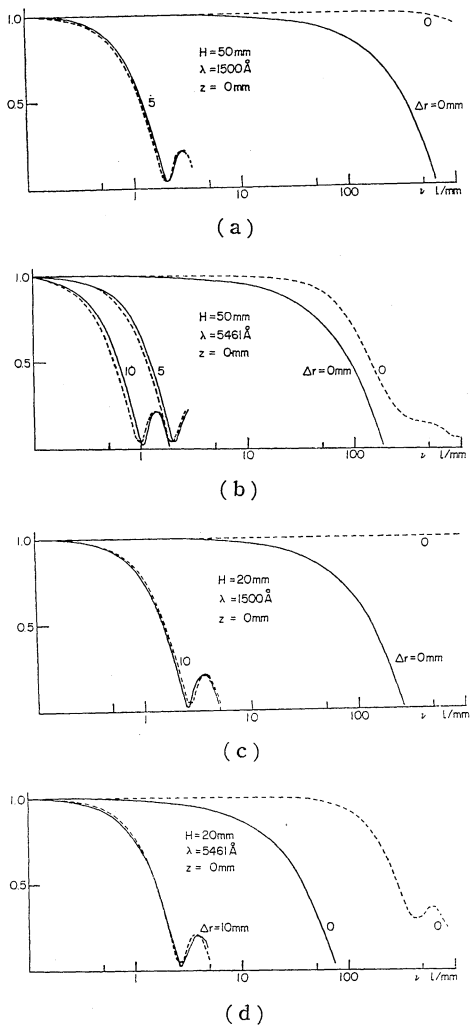

Fig. 6. Comparison of OTF based on wave optics (full line) and that on geometrical optics (dotted line) for Eagle mounting.

high spatial frequency.

§ 4. OTF as Fourier Transformation of Point Image

To check the above results, the OTF is calculated by the Fourier transformation of the intensity distribution of a point image. The intensity distributions of spectrometer image have been given by Stephan *et al.*[5] or by Namioka[4] for the Seya-Namioka mounting. Their results are transcribed in Fig. 8 (a) and (b) as full lines. According to their data, grating parameters are R=1000 mm, d=1/600 mm, C=70°15′ and m=−1. The units of the abscissae adopted in (a) and (b) correspond to $\Delta\lambda$=0.4A and $\Delta\lambda$=0.0426A respectively.

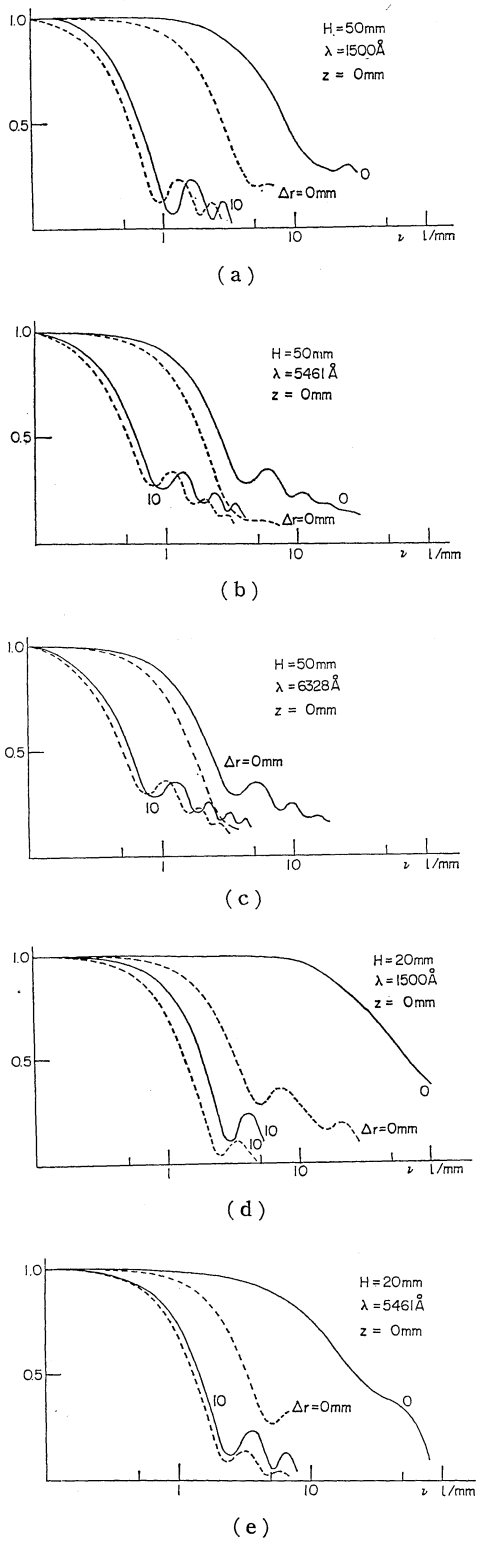

Fig. 7. Comparison of OTF based on wave optics (full line) and that on geometrical optics (dotted line) for Seya-Namioka mounting.

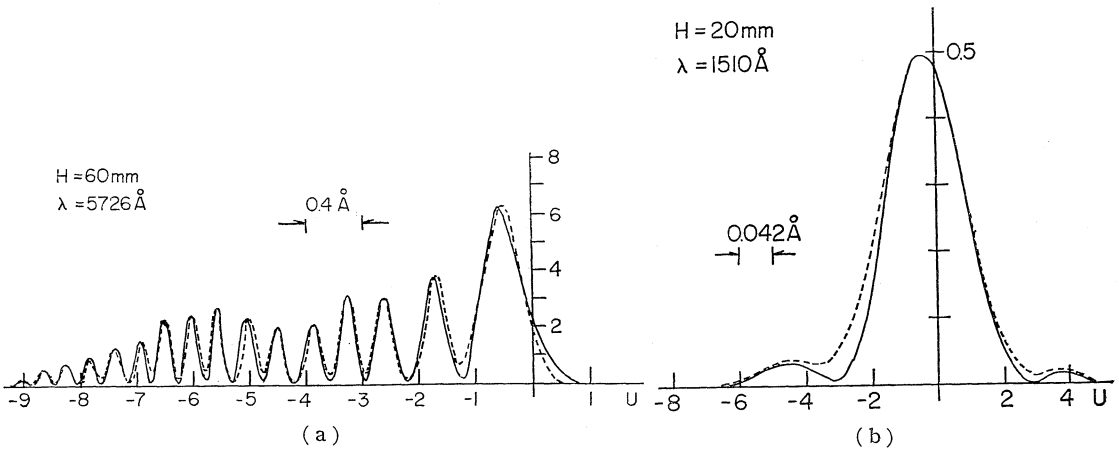

Fig. 8. Intensity distribution of point image for Seya-Namioka mounting (full line) and its approximation by superposition of many Gaussian functions (dotted line). Full lines are transcribed from the ref. 5) and 4).

These units in wavelength correspond to $\Delta u=14.5\mu$ and $\Delta u=1.33\mu$ respectively in the transverse distance at the image plane by the equation $\Delta u=r'\Delta\beta=mr'\Delta\lambda/d\cos\beta$.

A large number of intensity maxima are observed in the intensity distribution, and we represent them as a superposition of many Gaussian functions, each of which has the same half width and the maximum intensity as given in the literatures. The dotted lines in Fig. 8 (a) and (b) represent the curves plotted by using this approximation.

The Fourier transformation of the sum of the Gaussian functions shifted laterally by

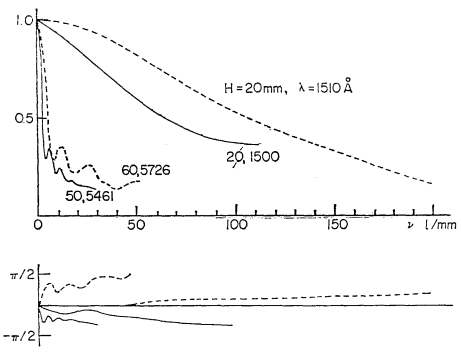

Fig. 9. Comparison of OTF by an autocorrelation of pupil function (full line) and OTF by Fourier transformation of intensity distribution of point image (dotted line).

u_n from the origin, $f(x)=\sum I_n\exp[-h_n^2(x+u_n)^2]$, is given by $F(\nu)=\sum(\sqrt{\pi}I_n/h_n)\exp[-\{(\pi\nu/h_n)^2+2\pi iu_n\nu\}]$. Then the OTF is given by

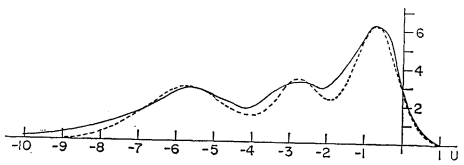

Fig. 10. Envelope of intensity maxima in Fig. 8 (a) (full line), and rewritten curve of the full line by the superposition of three Gaussian functions.

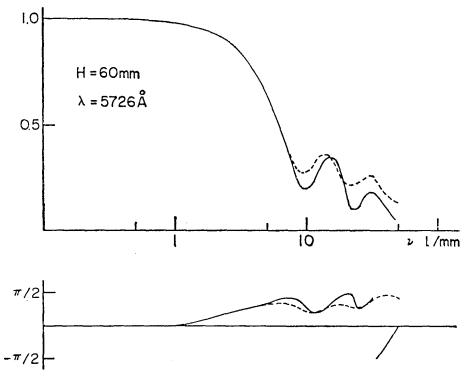

Fig. 11. OTFs obtained from the approximated curve of intensity distribution in Fig. 9 (full line) and from the exact curve in Fig. 8 (a) (dotted line).

$$|F(\nu)|=[\{\sum(I_n/h_n)\exp[-(\pi\nu/h_n)^2]\cos 2\pi u_n\nu\}^2+\{\sum(I_n/h_n)\exp[-(\pi\nu/h_n)^2]\times\sin 2\pi u_n\nu\}^2]^{1/2}/\sum(I_n/h_n). \quad (18)$$

Figure 9 shows a comparison of the OTF obtained from (18) and from (10). As there are some differences in the values of H, λ and C

between the data, and as the errors are introduced in reproduction of the small original curves of intensity distributions, the results are plausible. The discrepancy of phase is due to the opposite sign of diffraction order.

The full line in Fig. 10 represents an envelope of a large number of intensity maxima included in Fig. 8, and the curve is rewritten as the dotted line, which is obtained by a superposition of three Gaussian curves. If the intensity distribution can be approximated by this dotted line, the calculation becomes much easier. Figure 11 shows the OTF calculated by this approximation, and there is little difference between the curves with and without approximation. Therefore, when the OTF is obtained by the intensity distribution of the point image, the approximation such as Fig. 10 can be permitted.

References

1) H. G. Beutler: J. Opt. Soc. Amer. **35** (1945) 311.
2) H. Yoshinaga, B. Okazaki and S. Tatsuoka: J. Opt. Soc. Amer. **50** (1960) 437.
3) A. B. Shafer, L. R. Megill and L. Droppleman: J. Opt. Soc. Amer. **54** (1964) 879.
4) T. Namioka: J. Opt. Soc. Amer. **49** (1959) 951.
5) G. Stephan, J. C. Lemonnier et S. Robin: Optica Acta **12** (1965) 345.
6) A. Lohmann: Optica Acta **6** (1959) 175.
7) T. Katayama and A. Takahashi: Memoirs of the Defense Academy, Japan **7** (1967) 1055.
8) H. H. Hopkins: *Wave Theory of Aberrations* (Oxford) p. 22.
9) K. P. Miyake and T. Katayama: Sci. of Light (Japan) **11** (1962) 10.